Chapter 1

Introduction

In this thesis we investigate the large-scale configuration and dynamics of Saturn's magnetosphere, using *in situ* data and computer models. But first, we must consider the fundamental physics concepts that allow us to understand Saturn's magnetosphere, and the language we will use to describe it.

Saturn's magnetosphere comprises magnetic fields, electric fields and *plasma*. *Plasma* is considered the fourth state of matter after solid, liquid, and gas, and is formed of a gas that has been ionised, such that the atoms have been split up into negatively charged electrons and positively charged ions. Unlike neutral particles, charged particles are influenced by electric and magnetic fields, and this fundamentally determines how plasma behaves differently to other neutral states of matter. We therefore start this chapter with a discussion of how charged particles are affected by electromagnetic forces, and how we can understand these effects by considering the plasma as a bulk fluid. We then discuss the nature of the magnetised plasmas we encounter in space, moving outwards through the solar system from the Sun to Earth, Jupiter and finally Saturn. We provide details for the construction of a force-balance model of Saturn's *magnetodisc*, which is used throughout this thesis as a tool to explore the behaviour of Saturn's magnetosphere. We finish the chapter with a summary of the open questions in this area of research, some of which this thesis plans to address.

1.1 Physics of Magnetised Plasmas

1.1.1 Forces on an Individual Charged Particle

We begin with Maxwell's equations of electromagnetism. These are:

$$\nabla \times \boldsymbol{E} = -\frac{\partial \boldsymbol{B}}{\partial t} \tag{1.1}$$

$$\nabla \times \boldsymbol{B} = \mu_0 \boldsymbol{J} + \frac{1}{c^2}\frac{\partial \boldsymbol{E}}{\partial t} \tag{1.2}$$

$$\nabla \cdot \boldsymbol{E} = \frac{\rho_q}{\epsilon_0} \tag{1.3}$$

$$\nabla \cdot \boldsymbol{B} = 0. \tag{1.4}$$

These equations govern how electric ($\boldsymbol{E}$) and magnetic ($\boldsymbol{B}$) fields vary over time t and through space. $\boldsymbol{J}$ is the current density, ρ_q is the charge density, $c^2 = 1/\mu_0\epsilon_0$ is the square of the speed of light, and μ_0 and ϵ_0 are the constants known as the permeability and permittivity of free space. Together with the Lorentz force law, we can use these equations to understand how a charged particles interact with electric and magnetic fields. The Lorentz force is given by

$$\boldsymbol{F}_\mathrm{L} = q(\boldsymbol{E} + \boldsymbol{v} \times \boldsymbol{B}), \tag{1.5}$$

where q is the charge of the particle and $\boldsymbol{v}$ its velocity. In the absence of an electric field, and with a uniform magnetic field, it can be shown that this Lorentz force causes the charged particle to gyrate around the magnetic field direction, with angular frequency

$$\Omega_c = \frac{|q|B}{m} \tag{1.6}$$

known as the cyclotron frequency, where m is the mass of the particle and B is the magnitude of the magnetic field. From equation 1.5 with $\boldsymbol{E} = 0$, positively charged particles gyrate in a left-handed sense around the magnetic field, and negatively charged particles gyrate in a right-handed sense. The radius of this orbit is given by the gyroradius, or Larmor radius,

$$r_\mathrm{L} = \frac{v_\perp}{\Omega_c} = \frac{m v_\perp}{|q|B} \tag{1.7}$$

where $\perp$ and later $\parallel$ subscripts refer to components perpendicular and parallel to the magnetic field. r_{L} is generally larger for ions (which are more massive than electrons), and for particles with higher energy (and so higher $v_{\perp}$). Note that the Lorentz force acts perpendicular to the magnetic field by definition, and so the motion of charged particles *parallel* to the magnetic field is not affected by $\boldsymbol{B}$; charged particles are thus free to move up and down along magnetic field lines, in the absence of other forces.

In a spatially non-uniform magnetic field, a particle will not only gyrate around a magnetic field line, but the guiding centre of its gyratory motion will also drift, depending on the variation of the magnetic field. The velocity of this guiding centre motion is given by the gradient drift velocity

$$\boldsymbol{v}_{\mathrm{g}} = \frac{m v_{\perp} \boldsymbol{B} \times \nabla B}{2 q B^3} \tag{1.8}$$

and is therefore in a direction perpendicular to both the magnetic field direction and the gradient of the magnetic field magnitude. In an approximately dipolar magnetic field, e.g. at Saturn, the magnetic field strength decreases with radial distance, and so ∇B is oriented radially inwards, while the magnetic field $\boldsymbol{B}$ is oriented downwards near the equator (or upwards at other magnetised planets, such as Earth and Mercury). At Saturn, this has the net effect of causing positively charged ions to drift eastwards, and negatively charged electrons to drift westwards, which sets up a net flow of charge (i.e. current) eastwards, in the direction of planetary rotation.

In a dipolar magnetic field, the magnetic field lines are also curved, and so a charged particle moving freely along a magnetic field line will feel a centrifugal force. This force also induces a drift in the guiding centre of the charged particle's orbit, given by the curvature drift velocity

$$\boldsymbol{v}_{\mathrm{c}} = \frac{m v_{\parallel}^2 \, \boldsymbol{r}_{\mathrm{c}} \times \boldsymbol{B}}{q B^2 r_{\mathrm{c}}^2} \tag{1.9}$$

where $\boldsymbol{r}_{\mathrm{c}}$ is the radius of curvature vector for the magnetic field line, defined as pointing radially outwards from the centre of curvature to the particle. (As an example, for a dipole magnetic field $r_{\mathrm{c}} = r/3$ at the magnetic equator, where r

is the radial distance from the origin.) This therefore has the same effect as the gradient drift force, with ions drifting eastwards and electrons drifting westwards, resulting in a net current in the direction of planetary rotation at Saturn.

For a general external force $\boldsymbol{F}$ the guiding centre drift associated with that force is given by

$$\boldsymbol{v}_{\mathrm{F}} = \frac{\boldsymbol{F} \times \boldsymbol{B}}{qB^2}. \tag{1.10}$$

For the case $\boldsymbol{F} = q\boldsymbol{E}$, equivalent to the Lorentz force equation (1.5) in the absence of a magnetic field, then the q term on the denominator of equation (1.10) cancels, and $\boldsymbol{v}_{\mathrm{F}}$ is independent of q such that both electrons and ions drift in the same direction.

Finally, it is important to consider the phenomenon of magnetic mirroring of charged particles, as this dynamical effect is common in the approximately dipolar magnetic fields of magnetised planets. The magnetic moment μ_{m} of a charged particle gyrating in a circular orbit around a magnetic field with gyroradius r_{L}, can be written as

$$\mu_{\mathrm{m}} = \frac{mv_{\perp}^2}{2B} \tag{1.11}$$

from the definition $\mu = IA$, with $I = q\Omega_{\mathrm{c}}/2\pi$ and $A = \pi r_{\mathrm{L}}^2$. For a slowly varying magnetic field, this quantity is conserved and is known as the *first adiabatic invariant*. A consequence of this is that as a particle gyrates along a magnetic field line towards a region where the magnetic field strength increases (e.g. polar regions of a dipole magnetic field), the particle's perpendicular velocity $v_{\perp}$ must also increase, to keep μ_{m} constant. Without an external electric field to do work on the particle, the total energy of the particle $\frac{1}{2}m(v_{\perp}^2 + v_{\parallel}^2)$ must remain constant, and so an increase in $v_{\perp}$ coincides with a decrease in $v_{\parallel}$, until $v_{\parallel}$ reaches zero and the particle is 'reflected' back along the magnetic field line in the opposite direction. That is, the motion of the guiding centre of the particle motion reverses direction. This phenomenon causes charged particles to 'bounce' up and down along dipolar magnetic field lines, reflecting near the poles where the magnetic field strength acquires a value large enough to reverse the guiding centre motion.

Therefore, charged particles in a planetary dipole magnetic field simultaneously gyrate around the magnetic field lines, bounce up and down along them, and drift azimuthally around the planet in a direction depending on their charge.

1.1.2 Forces on a Collective Plasma

Considering the motion of individual charged particles can only get us so far when trying to understand the global dynamics of large-scale plasma structures, such as planetary magnetospheres. It can be helpful to describe the plasma as a single fluid, with a bulk plasma flow velocity $\boldsymbol{u}$. This approach is known as single fluid magnetohydrodynamics (MHD), and the *momentum equation* for the plasma fluid is given by

$$\rho \frac{d\boldsymbol{u}}{dt} = \rho_{\mathrm{q}} \boldsymbol{E} + \boldsymbol{J} \times \boldsymbol{B} - \nabla P + \rho \boldsymbol{g} \tag{1.12}$$

where ρ is the mass density of the plasma, P is the plasma pressure (assumed to be isotropic), and $\boldsymbol{g}$ is the acceleration due to gravity. The first terms on the right hand side correspond to the Lorentz force terms given in equation (1.5) for the bulk plasma. However if we assume quasi-neutrality, such that the density of ions and the density of electrons in the plasma are approximately equal, then ρ_{q} is negligible and we can ignore the effect of the electric field $\boldsymbol{E}$. This is appropriate when considering plasmas over large temporal or spatial scales, as the individual charged particles quickly adjust to remove any charge imbalance caused by local density variations. Similarly in most space plasmas we can neglect the gravitational term as being insignificant compared to other terms.

This leaves the plasma pressure gradient force and the $\boldsymbol{J} \times \boldsymbol{B}$ force as the dominant forces on the magnetised plasma. To understand the effect of the $\boldsymbol{J} \times \boldsymbol{B}$ force in particular on the plasma, it is helpful to consider the case where plasma flows are significantly slower than the speed of light, which is appropriate for space plasmas considered in this thesis. In this case, we can neglect the second 'displacement current' term in the Maxwell's equation known as the Ampère-Maxwell relation (equation 1.2), and so this simplifies to

$$\nabla \times \boldsymbol{B} = \mu_0 \boldsymbol{J}, \tag{1.13}$$

known as Ampère's Law. This allows the $\boldsymbol{J} \times \boldsymbol{B}$ force to be rewritten as

$$\boldsymbol{J} \times \boldsymbol{B} = -\nabla \left(\frac{B^2}{2\mu_0} \right) + \frac{1}{\mu_0} (\boldsymbol{B} \cdot \nabla) \boldsymbol{B}. \tag{1.14}$$

The first term on the right hand side corresponds to a magnetic pressure gradient

force, with magnetic pressure $P_{\mathrm{B}} = B^2/2\mu_0$. The second term on the right hand side corresponds to the magnetic tension force. The component of this force perpendicular to the magnetic field direction, known as the curvature force, acts to 'straighten' bent field lines, akin to the restoring force on a bent elastic band, and scales with the magnetic field strength and radius of curvature as B^2/r_{c}. The component of this force parallel to the magnetic field lines cancels out exactly with the parallel component of the magnetic pressure gradient force, as the total $\boldsymbol{J} \times \boldsymbol{B}$ force must act perpendicular to the magnetic field by definition.

We will return to these concepts of magnetic pressure and tension forces, and discuss force balance in the plasma in these terms throughout this thesis.

1.1.3 The Frozen-in Field Theorem

If we make a few more simplifying assumptions about the nature of our plasma, we have conditions for *ideal MHD*. In particular we assume the plasma conditions do not vary on length scales and time scales smaller than the particle gyroradius nor the associated gyroperiod. We also assume the conductivity of the plasma is sufficiently high that we can neglect Joule heating, resistivity and collisions between particles, which is appropriate for the collisionless space plasmas that we consider in this thesis. This leads us to the idealised Ohm's Law,

$$\boldsymbol{E} + \boldsymbol{u} \times \boldsymbol{B} = 0. \tag{1.15}$$

An important mathematical consequence of this is the *frozen-in field theorem*. This powerful theorem states, under the conditions as described above, that the plasma and the magnetic field are 'frozen in' to each other and move together. From equation (1.15) it can be shown that if a magnetic field threads through two plasma fluid elements, the field will continue to connect them even as the elements move and change shape and size. This also means that two different plasma populations embedded with different magnetic fields cannot mix.

This theorem is instructive in intuitively understanding the behaviour of many space plasmas, including planetary magnetospheres. To determine whether the evolution of a plasma is controlled by the magnetic field or the inertia of the plasma

itself, it is useful to consider the quantity plasma β, defined as

$$\beta = \frac{P}{B^2/2\mu_0}, \tag{1.16}$$

the ratio of the plasma to magnetic pressure. In high β ($>> 1$) regimes, the plasma pressure is dominant in determining the plasma behaviour, and the magnetic field that threads the plasma is approximately convected along with the plasma flow. In low β ($<< 1$) regimes, the opposite is the case; the magnetic field is sufficiently strong to resist deformation by the plasma pressure, and so instead the magnetic field determines the plasma flow direction, and the plasma is approximately locked into the magnetic field as it moves. Both regimes are found in space plasmas (discussed in the rest of this chapter), and we will encounter both regimes in our study of Saturn's magnetosphere in this thesis. In particular we will often refer to 'flux tubes' of plasma in Saturn's magnetosphere, which are volumes of plasma mapped out by the planetary magnetic field lines, and which generally obey this frozen-in condition.

When the magnetic field varies on length scales comparable to the gyroradius of the individual plasma particles, ideal MHD breaks down and the frozen-in field theorem no longer holds. In this case, we observe a phenomenon known as *reconnection*, where magnetic field lines (and their attendant plasmas) that were previously separated are forced close enough together that they reconnect across a very thin layer or boundary. This can cause an explosive release of plasma along the newly reconnected magnetic field lines, and a reconfiguration of the magnetic field. This is a fundamental process in planetary magnetospheres, and is discussed in more detail in Section 1.3.3.

1.1.4 Plasma Waves

Many different types of waves can be set up in magnetospheric plasma populations. If we assume these waves are small in amplitude and thus only cause first-order perturbations to the background plasma properties (represented by the subscript 0 in the following equations), then we can use MHD to characterise their propagation

speeds. The speed of sound in a plasma is defined as

$$c_{\rm s} = \sqrt{\frac{\gamma P_0}{\rho_0}}, \tag{1.17}$$

as for a classical gas, where γ is the ratio of specific heats. If we assume the plasma is incompressible, and *cold* such that $P_0 = c_{\rm s} = 0$, the MHD relations we have discussed can be used to derive the dispersion relation for the plasma:

$$\omega^2 = v_{\rm A}^2 k^2 \cos^2\theta \tag{1.18}$$

where ω is the wave angular frequency, k is the wave number and θ is the angle between the wave propagation direction and the background magnetic field direction, such that the term $k\cos\theta$ is the component of the wave vector parallel to the magnetic field. $v_{\rm A}$ is a characteristic speed known as the *Alfvén speed*,

$$v_{\rm A} = \frac{B_0}{\sqrt{\mu_0 \rho_0}}. \tag{1.19}$$

As shown by equation (1.18), the phase velocity depends on θ, and is maximum (equal to $v_{\rm A}$) for propagation parallel to the magnetic field, and vanishes to zero for propagation perpendicular to the field. The group velocity is aligned with the background magnetic field, and so energy is transmitted along the magnetic field direction for these *Alfvén* waves.

If instead we consider a *warm* plasma and include the effect of plasma pressure, this dispersion relation becomes

$$\frac{\omega^2}{k^2} = \frac{1}{2}\left(c_{\rm s}^2 + v_{\rm A}^2 \pm \sqrt{(c_{\rm s}^2 + v_{\rm A}^2)^2 - 4c_{\rm s}^2 v_{\rm A}^2 \cos^2\theta}\right) \tag{1.20}$$

where the $\pm$ introduces two different wave modes, known as the *fast* and *slow* modes. Fast mode waves arise when variations in the magnetic and plasma pressures are in phase, and slow mode waves arise when the variations are out of phase. While this dispersion relation may seem complicated, interesting results fall out when the parallel ($\cos\theta = 1$) and perpendicular ($\cos\theta = 0$) propagation cases are considered separately. In the limit of parallel propagation, the two wave modes propagate at the Alfvén speed $v_{\rm A}$ and the sound speed $c_{\rm s}$. For low β plasmas, $c_{\rm s} < v_{\rm A}$ and so

v_A is the velocity of the *fast* mode, while for high β plasmas the opposite is the case. In the limit of perpendicular propagation, the phase velocity of the *slow* mode vanishes to zero, and the *fast* mode propagates at the characteristic speed known as the *magnetosonic speed* c_{ms},

$$c_{ms} = \sqrt{v_A^2 + c_s^2}. \tag{1.21}$$

The group velocity is always aligned with the background magnetic field for the slow mode, but not for the fast mode, and so fast mode waves can transmit energy across the magnetic field direction.

Other types of waves can also be set up in magnetised plasmas, depending on the conditions. However for the magnetospheric plasma environments we discuss in this thesis, an understanding of the Alfvén, sound and magnetosonic speeds is sufficient.

1.2 The Solar Wind

The corona is the uppermost atmospheric layer of the Sun, and is composed mainly of ionised hydrogen (i.e. protons and electrons), with approximately 4% ionised helium (Robbins et al., 1970). This layer is heated from below by fusion processes in the deep interior, and other processes not yet fully understood, to extremely high temperatures of $\sim 10^6$K (Warren and Brooks, 2009). Above, the corona is surrounded by relatively empty space, and thus experiences a large thermal pressure gradient force directed radially outwards. This means that a significant fraction of the coronal plasma is energetic enough to escape the Sun's strong gravitational field, and thus streams radially outwards from the Sun through space at high speeds. This plasma flow is known as the solar wind.

The properties of the solar wind vary on many timescales; however, it is still useful to consider the typical properties. The typical solar wind speed is around $450\,\mathrm{kms}^{-1}$ throughout the solar system, well above the local speed of sound. The particle number density falls approximately as r^{-2} (the inverse square of radial distance from the Sun) in line with conservation of particle flux through an expanding spherical surface, with density from around $7\,\mathrm{cm}^{-3}$ at the orbit of Earth (1 AU) to $0.07\,\mathrm{cm}^{-3}$ at the orbit of Saturn (9.5 AU), where $1\,\mathrm{AU} = 1.496 \times 10^8\,\mathrm{km}$ (Bagenal et al., 2014). Near the solar surface, the strong and complex magnetic field of the

Sun dominates the coronal plasma, in line with the frozen-in field theorem for low β plasmas, and so generates phenomena such as coronal loops. However, further away from the Sun, beyond a few tens of solar radii, the magnetic field strength decreases with radial distance such that β increases, and the magnetic field becomes frozen-in to the moving solar wind plasma (Russell et al., 2016). The magnetic field is therefore carried outwards into space by the flowing plasma, where it is known as the interplanetary magnetic field (IMF). This radial outflow of the solar wind, combined with the ∼25 day rotation period of the Sun, produce a spiral-like distribution of magnetised plasma in the Sun's equatorial plane which extends throughout the solar system, known as the *Parker Spiral* (Parker, 1958). This structure influences the typical orientation of the interplanetary magnetic field observed at each planet, from approximately radial at the orbit of Mercury, to approximately perpendicular to the radial flow at the orbit of Saturn. Figure 1.1 shows a diagram of this phenomenon, created using values for the solar wind speed, solar rotation rate and planet orbit radii as quoted in this text. The orientation of the IMF has consequences for the interaction between the solar wind and the planet, as discussed in future sections.

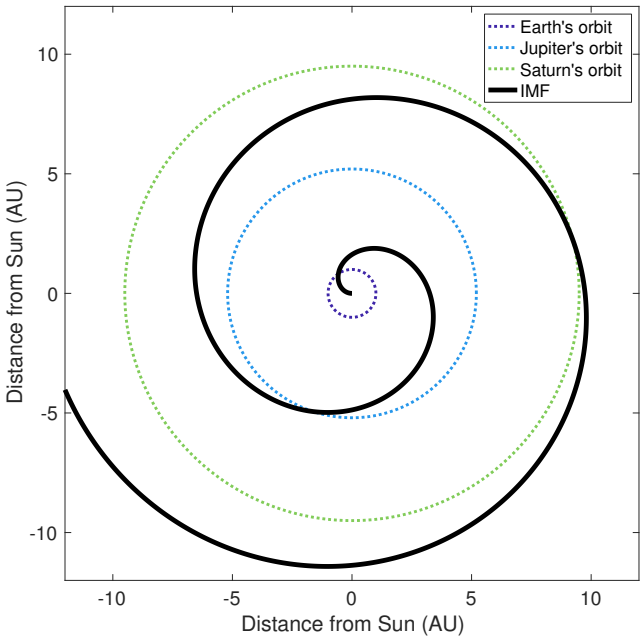

Figure 1.1: Diagram showing how the Parker Spiral affects the orientation of the IMF (interplanetary magnetic field) in the equatorial plane throughout the solar system. The orbits of different planets are shown by the coloured dotted lines.

On top of this rotating structure, the properties of the solar wind vary on

timescales ranging from minutes to years. At the shorter end of the time spectrum, coronal mass ejections (CMEs) are dynamic outflows of dense, coronal material that occur due to dramatic reconfiguration of the coronal magnetic field. These typically form over days and may reach speeds as high as several thousand kms^{-1} as they accelerate through the inner solar system (Russell et al., 2016). Their movements are associated with regions of enhanced density and magnetic field strength compared to the ambient solar wind (Odstrcil and Pizzo, 1999). At the opposite end of the spectrum, it is well known that the Sun exhibits periodic behaviour with an approximately 11 year cycle, known as the solar cycle. This cycle of alternatively high and low solar activity can be tracked well by the number of sunspots that appear on the solar surface, and is correlated with solar wind properties such as solar irradiance, magnetic field strength, and flare and CME incidences (Hathaway, 2015). There is therefore a great deal of variability in the magnetic and plasma environment of the solar system, over time and through space.

1.3 Planetary Magnetospheres

1.3.1 Structure of a Magnetosphere

A magnetosphere is a 'bubble' of magnetised plasma that surrounds a planet with a significant internal magnetic field, and forms due to the interaction between this magnetic field and the solar wind. Mercury, Earth, and the outer giant planets all have approximately dipolar internal magnetic fields, generated by convective flow of electrically conducting fluid in the planets' deep interiors; thus they all have stable magnetospheres (Kivelson and Bagenal, 2014).

As the solar wind flow is supersonic, a bow shock forms upstream of the magnetosphere obstacle. Downstream of this, the magnetosheath is the region between the bow shock and the magnetosphere proper, where the solar wind plasma is decelerated and deflected. The magnetopause is the surface that separates the internal planetary plasma of the magnetosphere, from the external shocked solar wind plasma of the magnetosheath.

In a steady state system, the shape and size of the magnetopause is determined by pressure balance across the boundary, between the internal magnetic and plasma pressures, and the external solar wind pressure. The magnetopause morphology in turn influences the configuration of the magnetosphere internally. Therefore, the

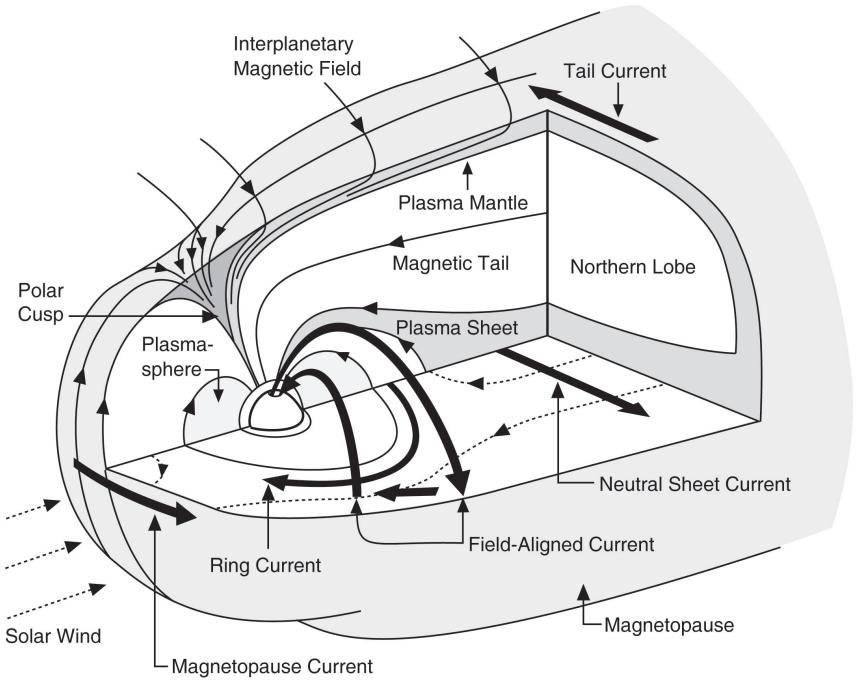

Figure 1.2: Diagram of the main features of Earth's magnetosphere from Russell et al. (2016), reproduced with permission.

structure of the magnetosphere varies significantly between different planets, where both the internal and external conditions are different. However, many features are broadly common to all planetary magnetospheres in some form, and Figure 1.2 shows a diagram specifically of Earth's magnetosphere, with these main features labelled. Note that at Jupiter and Saturn, the internal planetary magnetic field is oppositely oriented such that the magnetic fields and current systems are all in the opposite direction.

It can be seen that the magnetosphere is approximately dipolar in configuration on the dayside (i.e. the side facing the Sun), with a more extended 'tail' on the nightside (i.e. the anti-sunward side), where the magnetic field lines stretch radially outwards and become approximately parallel to the solar wind direction. This tail can extend to tens or hundreds of planetary radii downstream of the planet; Jupiter's magnetotail has even been observed to extend as far as the orbit of Saturn, corresponding to several thousand Jovian radii (Scarf et al., 1981). Figure 1.2 shows an azimuthal ring current system which orbits the planet, centred around the equatorial plane; the direction is determined by the direction of the curvature and gradient drift velocities for positively and negatively charged particles in Earth's

magnetic field, as described in Section 1.1.1 for the oppositely-oriented Saturn case. On the nightside this ring current extends into a current sheet, which separates the oppositely directed magnetic field lines in the northern and southern 'lobes' of the nightside magnetosphere. Currents also flow on the magnetopause and magnetotail surfaces as shown, separating the magnetic fields of the magnetosphere and the solar wind IMF. At the polar cusps, the magnetosphere is said to be 'open' to the solar wind, as in these regions the confined internal planetary dipole magnetic field structure changes in strength and direction over relatively small spatial scales, and so allows solar wind particles to access the magnetosphere. This is in contrast to the more 'closed' regions of the magnetosphere, where it is difficult for solar wind particles to penetrate.

1.3.2 Comparative Magnetospheres

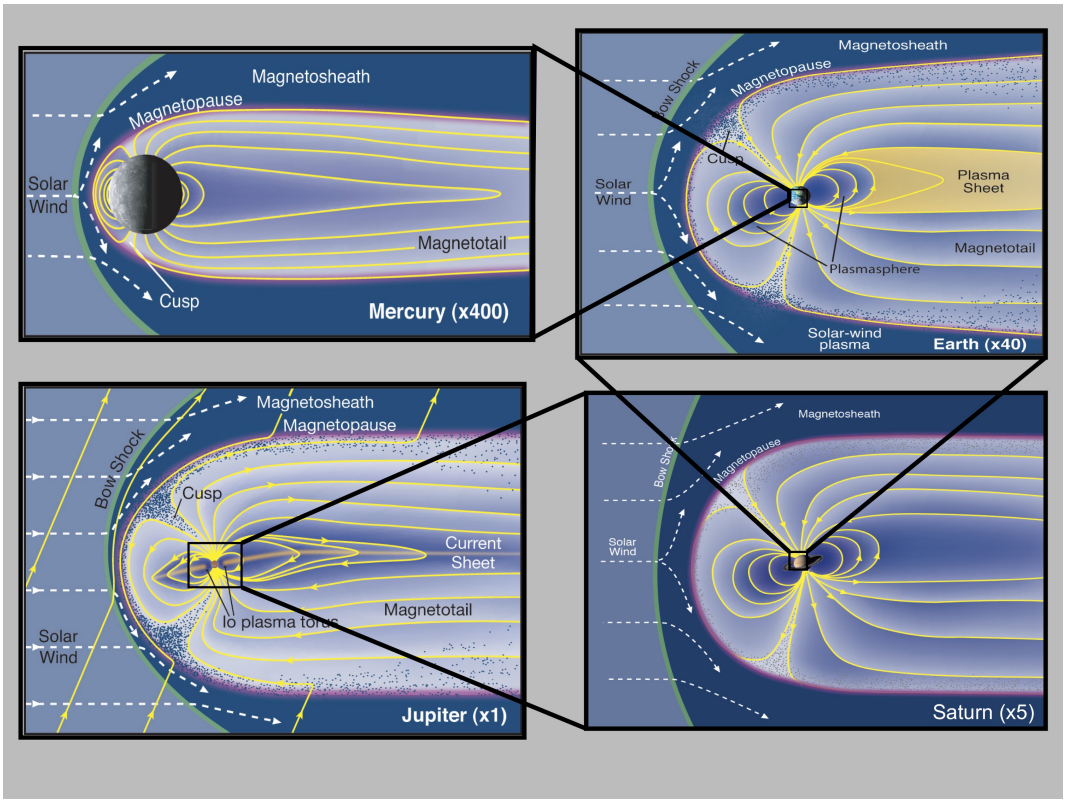

Figure 1.3: Diagram comparing the relative sizes and shapes of the magnetospheres of Mercury, Earth, Jupiter and Saturn, from Fran Bagenal and Steve Bartlett at LASP.

A comparison of the magnetospheres of different planetary systems is shown in Figure 1.3. The most striking difference is in the overall size of the magnetospheres, and this is mainly due to the twin influences of the external solar wind conditions at

Table 1.1: Comparison of typical magnetospheric parameters for Earth, Jupiter and Saturn, adapted from Bagenal et al. (2014) and references therein. $1\,\mathrm{AU} = 1.496 \times 10^8\,\mathrm{km}$ and $1\,\mathrm{M_{EARTH}} = 7.9 \times 10^{15}\,\mathrm{Tm}^3$.

	Earth	Jupiter	Saturn
Planet radius R_P (km)	6371	71 492	60 268
Distance from Sun (AU)	1	5.2	9.5
Solar wind number density (cm^{-3})	7	0.2	0.07
Spin period (hr)	24	9.9	10.6
Magnetic moment ($\mathrm{M_{EARTH}}$)	1	20 000	600
Equatorial surface magnetic field (nT)	30 600	430 000	21 400
Dipole stand-off distance R_CF ($\mathrm{R_P}$)	$10\,\mathrm{R_E}$	$46\,\mathrm{R_J}$	$20\,\mathrm{R_S}$
Observed stand-off distance R_MP ($\mathrm{R_P}$)	$8-12\,\mathrm{R_E}$	$63-92\,\mathrm{R_J}$	$22-27\,\mathrm{R_S}$

each planet, and internal magnetic pressure associated with the planetary magnetic field. Table 1.1 provides some typical parameters for the planets Earth, Jupiter and Saturn that help illustrate this. For example, the Jovian planetary dipole magnetic moment is some 20,000 times greater than that of Earth, with correspondingly higher magnetic field strength. This therefore means a much greater magnetic pressure inside Jupiter's magnetosphere. In addition, the solar wind dynamic pressure D_P is defined as

$$D_\mathrm{P} = \rho_\mathrm{m} u_\mathrm{SW}^2 \tag{1.22}$$

where ρ_m is the mass density of the solar wind and u_SW is the velocity. As discussed in Section 1.2, ρ_m falls approximately as r^{-2} while u_SW remains approximately constant, and so the external solar wind dynamic pressure is much lower for the planets in the outer solar system, falling as approximately r^{-2} . Therefore the solar wind dynamic pressure acting to compress the magnetosphere is much smaller at Saturn, and Jupiter, than it is at Earth.

This pressure-balance relationship is reflected in the 'dipole stand-off distance' R_CF for each planet given in Table 1.1, where CF stands for the derivation by Chapman and Ferraro (1930). This distance is a theoretical location of the magnetopause, measured from the planet centre to the sub-solar point on the magnetopause surface, which would be expected if the external solar wind dynamic pressure was balanced exactly by the magnetic pressure associated only with an internal *dipole* magnetic field. We can see that it is much greater for Jupiter and Saturn than for Earth, as expected from the pressure-balance explanation just given.

However, at Saturn and Jupiter in particular, the observed magnetopause stand-

off distances are significantly larger even than the Chapman-Ferraro estimates. This is mainly due to the significant internal plasma sources at each planet. At Saturn, the icy moon Enceladus orbits at a distance of $3.95\,R_S$, (where R_S is the radius of Saturn, 60 268 km) and ejects water group molecules into the magnetosphere at a rate of $\sim$150 kgs^{-1} (Tokar et al., 2006; Dougherty et al., 2006). At Jupiter, the volcanic moon Io orbits at $5.9\,R_J$ (where R_J is the radius of Jupiter, 71 492 km) and ejects sulphur dioxide into the magnetosphere at $\sim$1000 kgs^{-1} (Bagenal and Delamere, 2011). At each planet, this material is partially ionised, forming a torus of plasma around each planet. The plasma pressure associated with this population adds to the internal magnetic pressure, inflating the magnetosphere beyond the predictions of a vacuum dipolar internal field model. This is discussed in more detail in Section 1.4.2. In contrast at Earth, the Moon does not contribute a significant plasma population, and also mainly orbits the planet beyond the magnetosphere boundary, and thus does not have the same degree of influence on Earth's magnetosphere (e.g. Schneider, 1967).

For Jupiter and Saturn, these internal plasma populations not only influence the overall size of the magnetosphere but also the internal structure of the magnetic field. This is due to the rapid rotation rates of the two planets, shown by the short spin periods in Table 1.1. Due to the aforementioned frozen-in field theorem, the magnetospheric plasma is azimuthally accelerated towards co-rotation with the rapidly rotating magnetic field of the magnetosphere. The centrifugal force associated with this rotation confines the plasma towards the rotational equator, creating a plasma sheet. In order to balance this centrifugal force, the magnetic field is distorted about the plasma sheet from a dipolar magnetic field into a disc-like *magnetodisc* structure, with a strong associated magnetic curvature force. This structure is characterised by field lines that are stretched radially outwards near the equatorial plane in the outer magnetosphere (as can be seen particularly for Jupiter in Figure 1.3), and is supported by the azimuthal ring current. The intensity of the ring current is enhanced by a population of hotter, more variable plasma that originates in the outer magnetosphere at both Saturn (e.g. Sergis et al., 2010) and Jupiter (e.g. Mauk et al., 2004), with observed plasma β of the order $2-5$ and $\sim$100 for these populations respectively. These populations therefore further contribute to the formation of a

magnetodisc magnetic field structure at these planets. The magnetic field strength of the magnetodisc field structure in general varies more slowly with radial distance in the outer magnetosphere than a dipolar magnetic field, and thus also significantly influences pressure balance at the magnetopause. This behaviour is investigated for both Saturn and Jupiter in Chapter **??**.

1.3.3 Magnetospheric Dynamics

The simplest dynamical process that a magnetosphere undergoes is compression and expansion under varying solar wind conditions. For example, as the local solar wind dynamic pressure increases, due to an increase in velocity or number density by some process as described in Section 1.2, the magnetosphere becomes compressed. This compression causes the internal magnetic field pressure to increase, until (for steady state conditions) it balances the enhanced external solar wind dynamic pressure and a new equilibrium magnetopause location is reached. If the solar wind pressure decreases, the magnetosphere then inflates. The magnetopause is therefore in constant motion, with a velocity of order $10\,\mathrm{kms}^{-1}$ at Earth (Berchem and Russell, 1982) and $100\,\mathrm{kms}^{-1}$ at both Jupiter (Bame et al., 1992) and Saturn (Masters et al., 2011). The exact response of the magnetosphere to varying D_P varies significantly between planets due to the different internal structures. For Saturn in particular, the distance that the magnetopause location shifts for a given change in D_P, and how this varies with different internal and external conditions, is the subject of the study in Chapter **??**, and is discussed in detail there.

However, even under approximately constant solar wind conditions, a magnetosphere is not a static object. At the 'solar-wind driven' magnetospheres of Earth and Mercury, the dominant large-scale dynamic process is known as the *Dungey cycle*, after Dungey (1961). A diagram of this process is shown in Figure 1.4. For an IMF oriented anti-parallel to the planetary magnetic field, conditions are favourable for reconnection of the two magnetic fields at the dayside magnetopause, as the magnetic field varies on small spatial scales across the magnetopause boundary (as discussed in Section 1.1.3). The planetary magnetic field lines are then open to the solar wind at one end whilst still anchored to the planet at the other, and are thus convected by the solar wind flow downstream to the nightside. This leads to a build-up of magnetic flux on field lines in the magnetotail, which then reconnect across

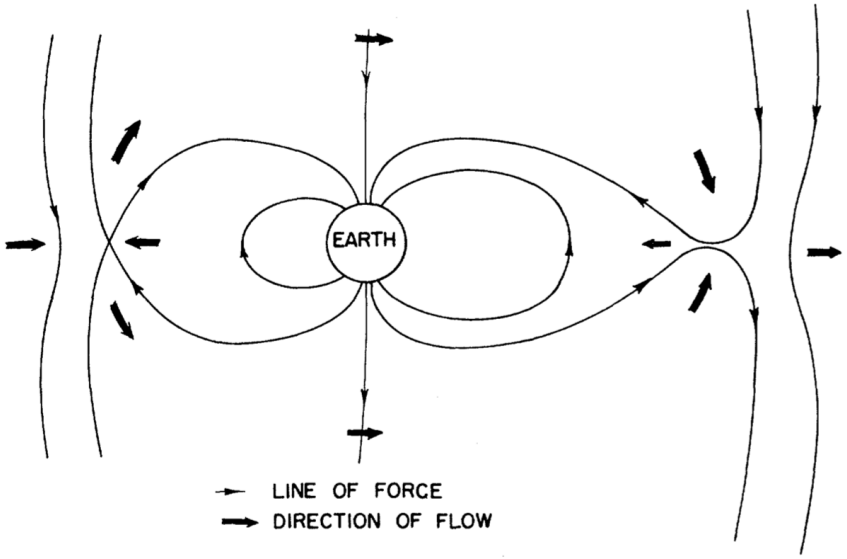

Figure 1.4: Diagram showing the Dungey cycle process at Earth, from Dungey (1961). Thin black 'lines of force' are magnetic field lines. The solar wind flows from left to right.

the tail current sheet. This causes plasma to accelerate and return on closed field lines back towards the planet on the nightside. At Earth, this process is associated with the generation of aurora along the boundary between open and closed magnetic field lines, in the northern and southern polar atmospheres (e.g. Milan et al., 2007). As the energetic electrons in the plasma gyrate around the polar magnetic field lines and move towards the planet, they excite atoms in the atmosphere, which then decay back to their lower energy levels and emit photons in the process. These are observed as auroral emissions.

At Jupiter and Saturn, the dominant dynamical process which causes a large-scale reconfiguration of the magnetic field is internally driven by the rapid planetary rotation, and thus we say they are 'rotationally driven' magnetospheres. This process is known as the *Vasyliunas cycle*, after Vasyliunas (1983), and a diagram depicting it is shown in Figure 1.5. As discussed in the previous section, these rapidly rotating magnetospheres have significant internal plasma populations, which are accelerated to near-corotation with the rotating planetary magnetic field. The centrifugal interchange instability causes this plasma to be transported radially outwards, such that inner cold, dense flux tubes are exchanged with outer hot, tenuous flux tubes (Southwood and Kivelson, 1989), and the magnetic field is stretched out as shown in region 1 of Figure 1.5. As the flux tubes rotate around to the nightside, they are no

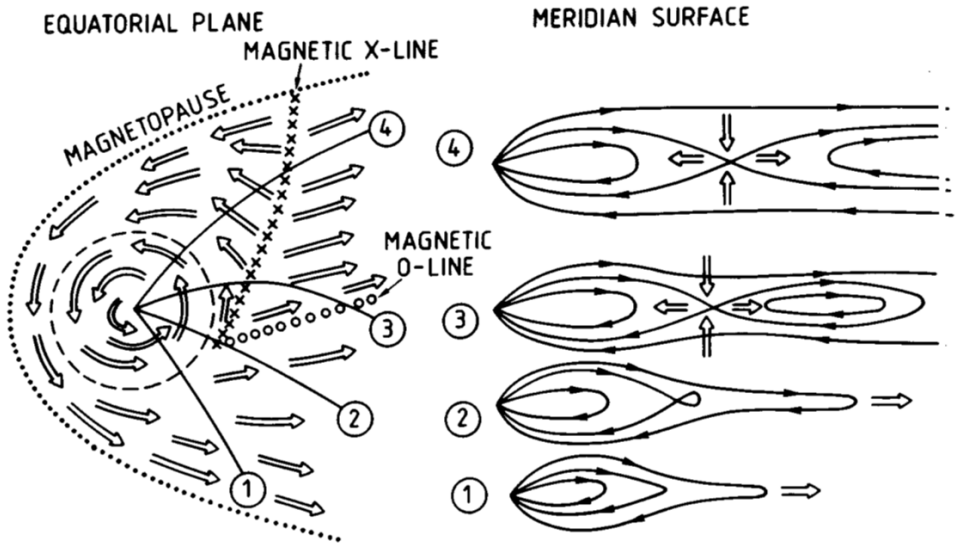

Figure 1.5: Diagram showing the Vasyliunas cycle of plasma transport, from Vasyliunas (1983). The dotted line shows the magnetopause boundary, the dashed line shows the region where plasma perfectly corotates with the magnetic field, and empty arrows show the plasma flow direction.

longer as confined by the magnetopause boundary and so expand down the tail, and the magnetic field becomes increasingly more stretched (region 2) until reconnection occurs across the tailward portion of the flux tube (region 3). This generates the release of a *plasmoid* down the tail, and the newly empty flux tube is then convected back around the planet via the dawn side.

This cycle is dominant over the Dungey cycle for the outer giant planets due to the combined effects of the much faster rotation rates, and overall larger magnetospheric sizes, which means a much longer period of time for a magnetic field line to be convected across the polar cap from dayside to nightside (Forsyth et al., 2010). However at Saturn in particular, it still uncertain how much of a role the Dungey cycle has to play in magnetospheric dynamics (e.g. Cowley et al., 2005). In particular, Saturn's aurora are thought to have an 'Earth-like' origin, associated with flow shear at the boundary between open and closed magnetic field lines. We discuss this further in Chapter **??**.

In addition to these main modes of plasma transport in planetary magnetospheres, there are also numerous small-scale dynamical processes, such as Kelvin-Helmholtz vortices on the magnetopause surface; however these vary significantly between planets and are not relevant to the work of this thesis, and so we do not cover them explicitly here.

1.4 Saturn and its Magnetosphere

Saturn orbits the Sun once every ∼29 years, on an elliptical orbit at an average distance of 9.5 AU. Saturn is approximately 10 times the size of Earth (by radius), and around 100 times as massive, meaning its density is around 1/10 of Earth's. This is because Saturn is a 'gas giant' planet, composed mainly of molecular hydrogen and helium, with a small rocky core. Between the core and the outer layers, the hydrogen is compressed to such high pressures and temperatures that it becomes 'metallic', flowing and conducting electricity and generating the dynamo of Saturn's planetary magnetic field.

The internal planetary magnetic field is approximately dipolar, though with smaller higher order moments. It may be approximated by a dipole offset northwards from the planetary equator by $\sim 0.05\,R_S$ (Dougherty et al., 2018). Arguably the most interesting aspect of Saturn's internal magnetic field is that the dipole axis is extremely closely aligned with the planet spin axis, with the same study by Dougherty et al. (2018) finding an upper limit of 0.01° difference between them. This is seemingly in contradiction with Cowling's Theorem, which states that an active dynamo cannot maintain a perfectly axisymmetric magnetic field (Cowling, 1933). This extreme axisymmetry also means it is nearly impossible to determine the rotation rate of the planet's deep interior from magnetic field measurements; however, a range of periodic phenomena are observed at Saturn, at periods assumed *close* to the true planetary rotation rate, as discussed in detail in Section 1.4.1.

From Table 1.1 and the associated discussion, we have seen that in many ways Saturn's magnetosphere is an intermediate case between Earth and Jupiter. It is therefore a particularly interesting system to study, and can be used to learn more about magnetospheric physics in a global context. Saturn's magnetosphere was first investigated *in situ* with single flybys by the outer solar system space missions *Pioneer* (1979), *Voyager 1* (1980) and *Voyager 2* (1981). These observations did not reveal a significant magnetodisc magnetic field structure on Saturn's dayside (as was known to exist at Jupiter), although did provide some evidence for a thin current sheet on the dawn flank (Smith et al., 1980). However with the arrival of the *Cassini* space mission into orbit around Saturn in 2004, and its continued observation of the system until late 2017, our scientific understanding of Saturn's

magnetosphere has been revolutionised. (The *Cassini* space mission is discussed in detail in Chapter **??**.)

We now know that in the outer magnetosphere, a non-negligible magnetodisc magnetic field structure typically exists at all local times beyond a radial distance of $\sim$15 R_S, due to the reasoning discussed in Section 1.3.2. However particularly on the dayside near noon, it was found that a significant magnetodisc structure only forms under relatively low solar wind dynamic pressure, when the subsolar magnetopause stand-off distance becomes greater than $\sim$23 R_S. When the magnetosphere is more compressed than this, the magnetic field near noon is approximately dipolar (Arridge et al., 2008). A study by Bunce et al. (2008) based on ring-current modelling found similar behaviour. It is interesting that this threshold value of $\sim$23 R_S falls between the two modes of the bimodal distribution in magnetopause stand-off distances observed by Achilleos et al. (2008) and Pilkington et al. (2015a), of 21 R_S and 27 R_S. This transition between a dipolar and disc-like field is broadly due to overall force balance in Saturn's magnetosphere; for a more expanded system, the magnetic field strength is weaker in the outer magnetosphere, and so a larger magnetic tension force (i.e. a more curved field line structure) is needed to balance the centrifugal and plasma pressure gradient forces acting radially outwards on the plasma. In Chapter **??** of this thesis, we present theoretical results that show the compressibility of the magnetosphere also changes behaviour at around this value of stand-off distance, at $\sim$25 R_S.

The formation of a magnetodisc structure at Saturn is also influenced by the variable hot plasma population observed by Sergis et al. (2010) and others, as discussed in Section 1.3.2, through an enhancement of the equatorial ring current intensity. By consideration of Ampère's law, it can be understood that the magnetic field associated with an azimuthal current flowing in the direction of corotation decreases Saturn's planetary magnetic field in the inner magnetosphere, and increases it in the outer magnetosphere. This is an important aspect of a magnetodisc magnetic field structure. Many studies have attempted to characterise the thickness and radial extent of this equatorial ring current at Saturn, using a combination of *Cassini* data, and models such as those of Connerney et al. (1981, 1983); Bunce et al. (2007), which assume an azimuthally symmetric current loop of uniform thickness and rectangu-

lar cross section. Saturn's ring current properties have been observed to vary over time, with location, and with system size (e.g. Bunce et al., 2007), with a variable typical half-thickness of $\sim 2\,R_S$ and significant radial extent, from around $7\,R_S$ out to around $18\,R_S$, at times reaching the magnetopause boundary on the dayside (e.g. Kellett et al., 2009; Sergis et al., 2009). However due to incomplete coverage across local time for most of the *Cassini* mission, it was not until near the end of the mission that the local time asymmetry of the ring current was demonstrated by Sergis et al. (2017). Indeed, the local time variation in the large scale structure of Saturn's magnetosphere is still not fully understood, and is studied and characterised further in this thesis in Chapter **??**, using a flexible model of the ring current adapted from Achilleos et al. (2010a), known as the UCL/AGA model. This model is discussed in Section 1.5.

1.4.1 Near-Planetary-Period Periodicities in Saturn's Magnetosphere

Another key aspect of Saturn's magnetosphere that is still not fully understood, is the nature of the observed periodic variations in field and particle properties. These variations, summarised in Carbary and Mitchell (2013), have periods ranging from around 10.6-10.8 hours, assumed close to the true planetary rotation rate. Magnetospheric periodicities have been found in the location of the auroral oval (Provan et al., 2009), and the magnetopause boundary (Clarke et al., 2010); the magnetic field strength and direction (Espinosa and Dougherty, 2000; Andrews et al., 2008); electron densities (Morooka et al., 2009); ion distributions (Burch et al., 2009); and energetic neutral atoms (Paranicas et al., 2005). These observations are especially interesting due to the aforementioned axisymmetry of Saturn's magnetic field, which means they cannot be adequately explained by a geometric tilt of the magnetic field. In addition, some of the observed periods vary relatively quickly, by up to 1% over the course of a year, and thus cannot be associated with changes to the planet's deep interior. This complex behaviour is apparently unique to Saturn, and has made it impossible directly to measure Saturn's true 'core' rotation rate.

Initially, periodicities in radio observations of Saturn's auroral regions from the *Voyager* spacecraft suggested a planetary rotation period of 10.657 h (Desch and Kaiser, 1981). This radio emission is known as Saturn Kilometric Radiation,

or SKR. Observations from the *Ulysses* (Lecacheux et al., 1997) and later *Cassini* (Gurnett et al., 2005) missions revealed that the SKR period was actually drifting over time, and thus could not be associated with the core rotation rate. A reanalysis of magnetometer data from the *Voyager* and *Pioneer* missions then showed a similar periodic behaviour in the magnetic field (Espinosa and Dougherty, 2000). This led to the development of a 'camshaft' model, where a rotating equatorial magnetic anomaly that is fixed in longitude triggers radial waves that cause the observed perturbations (Espinosa et al., 2003). To further complicate the picture, two distinct periods were then discovered in the SKR signal in the *Cassini* data, associated separately with the Northern and Southern hemispheres (Gurnett et al., 2009). This phenomenon was then also observed in more recent *Cassini* magnetic field observations (e.g. Andrews et al., 2010; Provan et al., 2012). In these and other studies, such as Hunt et al. (2014), a picture has now been developed of how these hemispheric magnetic perturbations are generated, by two large-scale field-aligned current systems that rotate at slightly different rates in each hemisphere. The magnetic field associated with each current system is dominant in the respective hemisphere, and can be approximated in the outer magnetosphere by a rotating, transverse oriented dipole. However the true magnetic field perturbation is much more complex, and is currently an area of active research, with some final *Cassini* results still to be fully analysed. The physical origins of these current systems are also still not fully understood, but are thought to be associated with twin atmospheric vortices flowing in the polar upper atmosphere/ionosphere in each hemisphere (Jia and Kivelson, 2012; Southwood and Cowley, 2014; Smith et al., 2016).

In the equatorial plane, these magnetic field perturbations have the effect of making Saturn's current sheet appear to'flap' above and below the rotational equator once per planetary rotation (e.g. Arridge et al., 2011). Similar behaviour is also observed at Jupiter (e.g Khurana and Kivelson, 1989); however at Jupiter the dipole axis is tilted 9.4° relative to its rotation axis, which means that relative to the rotational equator, the current sheet behaves approximately as a rotating, tilted disc, and so this behaviour is expected. In addition, at Saturn, these periodic magnetic field perturbations have the effect of periodically thickening and thinning the current sheet at different longitudes (Provan et al., 2012), associated with a large scale com-

pression and expansion of the magnetosphere in a given region, known as 'breathing' (Ramer et al., 2017). Both the 'flapping' and 'breathing' behaviours are controlled by the relative phases of the northern and southern magnetic perturbations, noting that their independent rotation rates cause the phase relationship between them to change over time, known as beating. This complicated dynamical behaviour is the focus of much current research, and is the subject of the study in Chapter **??**.

1.4.2 Pressure Balance at Saturn's Magnetopause

As previously mentioned, the magnetopause boundary can be approximated as the location where the effective pressure of the solar wind exerted on the magnetosphere is exactly balanced by the sum of the internal magnetospheric particle and field pressures.

Before impacting on the magnetopause, the solar wind flow is first decelerated via the bow shock, and is deflected around the magnetosphere obstacle. This acts to reduce the dynamic pressure incident on the magnetopause surface, and must be accounted for when considering pressure balance. Petrinec and Russell (1997) used Bernoulli's equation in combination with the Rankine-Hugoniot jump conditions across the bow shock, assuming adiabatic flow of the solar wind, to show that the relation

$$\frac{B_{\mathrm{MS}}^2}{2\mu_0} + P_{\mathrm{MS}} = kD_{\mathrm{P}} \cos^2\psi + P_0 \sin^2\psi \tag{1.23}$$

provides an approximation that is valid across the magnetopause surface, not just at the nose. The subscript MS denotes magnetospheric properties, such that the terms on the left hand side of equation (1.23) are the magnetospheric magnetic and plasma pressures respectively. ψ is the flaring angle measured between the upstream flow velocity vector and the normal to the magnetopause surface, such that $\psi = 0$ at the nose and generally increases as you move anti-sunward along the magnetopause surface. The first term on the right hand side is associated with the solar wind dynamic pressure D_{P}, where k is a positive constant ≤ 1 to account for the aforementioned diversion of flow, and the $\cos^2\psi$ factor accounts for the reduction in the normal component of dynamic pressure on the flanks and tail of the magnetosphere. The second term on the right hand side is composed of a 'static' pressure P_0 associated with the thermal pressure of the solar wind, and a $\sin^2\psi$ factor to ensure a real (i.e. not imaginary) flow velocity in the subsolar region (see

Petrinec and Russell, 1997).

In order to improve agreement with the results of MHD simulations from Hansen et al. (2005), and to improve the consistency of D_{P} estimates, Kanani et al. (2010) proposed a modification to this relation such that P_0 is dependent on D_{P}. The relationship then becomes

$$\frac{B_{\mathrm{MS}}^2}{2\mu_0} + P_{\mathrm{MS}} = \left[k\cos^2(\psi) + \frac{k_{\mathrm{B}}T_{\mathrm{SW}}}{1.16 m_{\mathrm{p}} u_{\mathrm{SW}}^2}\sin^2(\psi)\right] D_{\mathrm{P}} \tag{1.24}$$

where k_{B} is the Boltzmann constant, m_{p} is the mass of a proton, and T_{SW} and u_{SW} are the solar wind temperature and velocity respectively. The value of k depends on the ratio of specific heats γ in the solar wind, and the upstream sonic Mach number M. For high ($\gtrsim$8) Mach number flow with $\gamma = 5/3$, $k = 0.881$ (Spreiter et al., 1966), which is a valid assumption for the solar wind at Saturn's orbit (e.g. Slavin et al., 1985; Achilleos et al., 2006). In Pilkington et al. (2015a), the authors use values of $k_{\mathrm{B}}T_{\mathrm{SW}} = 100\,\mathrm{eV}$ and $u_{\mathrm{SW}} = 460\,\mathrm{km\,s^{-1}}$ to represent typical solar wind conditions at Saturn; we use the same values in this thesis when we utilise this relation.

This relation allows an approximation of the solar wind dynamic pressure to be made, when only internal information about the state of the magnetosphere is known. Thus this relation is often used in studies that attempt to model the shape and size of the magnetopause boundary in response to changing D_{P}, using only *in situ Cassini* data for the magnetic and plasma pressure inside the magnetosphere. These studies are discussed in more detail in Chapter **??**.

1.5 The UCL/AGA Force-Balance Model of Saturn's Magnetodisc

Throughout this thesis we will employ the University College London/Achilleos-Guio-Arridge (UCL/AGA) magnetodisc model from Achilleos et al. (2010a,b), with appropriate modifications as described in each chapter. This model is based on a magnetic field and plasma model originally constructed for the Jovian magnetodisc by Caudal (1986), and adapted for the Saturn system. More information can be found in Achilleos et al. (2010a,b). The model is axisymmetric about the planetary dipole/rotation axis, which are assumed to be parallel. This parallel assumption is

appropriate for Saturn in particular, as the rotation and dipole axes are aligned to within 0.01° (Dougherty et al., 2018). This axisymmetric assumption is appropriate as an approximation of the large-scale structure of the magnetic field, as shown by Hunt et al. (2014), who compared the gradients of currents in radial, azimuthal and meridional directions and found the azimuthal gradients could be neglected. It is constructed based on the assumption of force balance in the rotating plasma of the magnetosphere between the Lorentz body force (including magnetic pressure and tension forces), pressure gradient force and centrifugal force, such that

$$\boldsymbol{J} \times \boldsymbol{B} = \nabla P - n m_i \omega^2 \rho \hat{\boldsymbol{\rho}} \tag{1.25}$$

where ρ is cylindrical radial distance from the axis, with $\hat{\boldsymbol{\rho}}$ its unit vector. The plasma properties are isotropic pressure P, temperature T, ion number density n, mean ion mass m_i and angular velocity ω. Note that this construction is equivalent to equation (1.12), the MHD momentum equation from Section 1.1.2 (with simplifying assumptions as described in that section), assuming force balance such that the acceleration of the plasma is zero, and including the centrifugal force on the plasma associated with the planetary rotation, for a frame of reference that corotates with the plasma.

As a consequence of Maxwell's equation (1.4), any magnetic field can be presented in terms of two Euler potentials α and ξ, such that

$$\boldsymbol{B} = \nabla\alpha \times \nabla\xi. \tag{1.26}$$

For an axisymmetric field with no azimuthal component, the forms of α and ξ can be chosen such that all the information about the poloidal magnetic field is contained in one Euler potential which we call $\alpha = \alpha(r, \mu)$, where r is radial distance from the origin, and $\mu = \cos\theta$, the cosine of colatitude. Using this form of α, Caudal (1986) demonstrated that equation (1.25) is equivalent to the partial differential equation

$$\frac{\partial^2\alpha}{\partial r^2} + \frac{1-\mu^2}{r^2}\frac{\partial^2\alpha}{\partial\mu^2} = -g(r, \mu, \alpha) \tag{1.27}$$

in normalised units (see Achilleos et al., 2010a, for details), where $g(r, \mu, \alpha)$ is a

source function determined by the distribution of plasma and angular velocity in r, μ space. This equation can be solved semi-analytically using Jacobi polynomials as laid out in detail in Achilleos et al. (2010a, Appendix) to give surfaces of constant α, corresponding to magnetic field lines, in r, μ space. The solution also provides a prediction of the local plasma pressure, and the azimuthal current density components associated with each of the terms on the right hand side of equation (1.25).

Since the source function is itself dependent on α, equation (1.27) must be solved iteratively, starting from a pure dipole magnetic field and then successively perturbing it. At each iteration, a linear combination of the present solution α_i and the previous solution α_{i-1} is used as input for the next iteration calculation, such that

$$\alpha_{i+1(\mathrm{input})} = \gamma\alpha_i + (1-\gamma)\alpha_{i-1}, \tag{1.28}$$

where $\gamma < 1$ controls the relative weighting between the previous and current solutions. This is a form of numerical relaxation which stabilises the approach to the equilibrium solution. This $\alpha_{i+1(\mathrm{input})}$ is then used to calculate the source function in equation (1.27) to solve for α_{i+1}. In the original model construction, the two components were weighted equally ($\gamma = 0.5$) and calculations continued until the maximum relative difference between successive iterations fell below a chosen 'tolerance' $\delta = 0.5\%$, considered as convergence. In some of the work in this thesis we found that, for models with more extreme input parameters, it was necessary to weight the previous solution up to nine times more heavily than the present solution ($\gamma = 0.1$), in order to achieve convergence. (Exactly what constitutes an 'extreme parameter' will be discussed in future chapters.) In order to keep the ratio δ/γ constant at 10^{-2}, and therefore consistent with the original model approach, this corresponds to using a more stringent stopping tolerance $\delta = 10^{-2} \times 0.1 = 0.1\%$ in such cases.

The global plasma properties can then be inferred entirely from the calculated magnetic field structure, using appropriate boundary conditions, as follows. Caudal (1986) explained that as a consequence of equation (1.25), with T and ω constant along magnetic field lines (according to Liouville's theorem and Ferraro's isorotation

theorem respectively), the plasma pressure P is determined by

$$P = P_0 \exp\left(\frac{\rho^2 - \rho_0^2}{2\ell^2}\right), \tag{1.29}$$

where ℓ is the *confinement scalelength* (in ρ)

$$\ell^2 = \frac{2k_B T}{m_i \omega^2}. \tag{1.30}$$

The subscript 0 means the quantity evaluated at the equatorial crossing point of the magnetic field line. This represents the plasma being confined towards the rotational equatorial plane due to the centrifugal force exerted on it. Again, this is in normalised units as described in Achilleos et al. (2010a), so ℓ has units of R_S here. The model assumes that the plasma is composed of a cold and hot population; for the hot plasma population, the thermal energy associated with the plasma is significantly greater than the centrifugal potential, and so ℓ^2 tends to infinity, such that the hot plasma pressure is not confined to the equator but is constant along magnetic field lines, $P_H = P_{H0}$. This assumption is supported by observations such as Krimigis et al. (2007), who used data from the *Cassini* MIMI instrument to show that the hot plasma population extends to high latitudes, particularly on the dayside, verifying that the plasma can effectively fill their flux tubes due to their high energies. Similarly, a recent study by Sergis et al. (2018) showed that the UCL/AGA model with this assumption accurately predicts the relationship between high latitude and equatorial hot plasma pressure distributions. Hence, the full form of equation (1.29) is only necessary for calculating the cold plasma pressure.

The requisite boundary conditions for the model are, then, the equatorial radial profiles of the relevant plasma properties. These were obtained from studies using results mainly from *Cassini* plasma instruments CAPS and MIMI/INCA, as summarized in Achilleos et al. (2010a), and updated in Achilleos et al. (2010b). (These *Cassini* instruments are described in detail in Chapter **??**.) For the cold plasma population, the profiles for m_i and T were obtained using results from Wilson et al. (2008), ω profiles from Wilson et al. (2008) and Kane et al. (2008), and the flux tube content information from McAndrews et al. (2009). For the studies described in Chapters **??** and **??** we updated some of these boundary conditions using more

recent results from Wilson et al. (2017), as described in those chapters, with details in the Appendix **??**.

As the hot plasma pressure is assumed uniform along magnetic field lines, the plasma population may be completely characterised by a particular equatorial plasma pressure P_{H0} and flux tube volume V per unit of magnetic flux, where

$$V = \int_0^{s_B} ds/B, \tag{1.31}$$

and ds is an element of arc length along the magnetic field line. The integral limits represent measurement along a field line of total length s_B between the southern and northern ionospheric footprints at $1\,\mathrm{R_S}$. The flux tube volume is therefore dependent on both the shape of magnetic field lines, via ds, and the strength of the field, via B. Studies using *Cassini* MIMI data such as Sergis et al. (2007) found that the equatorial pressure associated with the hot plasma population was highly variable with ρ and over time, as described in Section 1.4. In light of these observations, the original Achilleos et al. (2010a) model simply parameterised the global hot plasma content by a single 'hot plasma index' K_{H}, where $K_{\mathrm{H}} = P_{\mathrm{H0}}V$ is constant beyond $8\,\mathrm{R_S}$, and P_{H0} decreases linearly to 0 inside that distance. A similar parameterisation, though with different values of the constants, was made in Caudal (1986), who argued that for the Jovian system, under the expected conditions of rapid radial diffusion, the hot plasma would be transported isothermally. In Achilleos et al. (2010a) the authors used a value of $K_{\mathrm{H}} = 2 \times 10^6\,\mathrm{Pa\,m\,T^{-1}}$ to represent just above 'typical' hot plasma content conditions at Saturn, although results presented in that study suggest K_{H} may vary in the range $10^5 - 10^7\,\mathrm{Pa\,m\,T^{-1}}$. Parameterising the hot plasma content by this single hot plasma index provides the flexibility to very simply characterize the level of ring current activity in the model, and thus investigate the effect of the varying hot plasma content on magnetospheric structure, and magnetospheric compressibility. This is the basis of the study described in Chapter **??**. In that chapter we also consider the consequences of modifying the definition of K_{H} to correspond to adiabatic plasma transport. In Chapter **??**, this hot plasma pressure boundary condition is updated to describe different local time sectors, using recent results from Sergis et al. (2017).

Finally, at every iteration, a small, uniform, southward-directed 'shielding field'

is added to the magnetic field, in order to approximately account for the magnetic field associated with the magnetopause and magnetotail current sheets. Sketches of these current systems are included in the diagram in Figure 1.2, though note they are in the opposite sense for the Saturn system due to the opposite orientation of Saturn's planetary dipole. In Achilleos et al. (2010a) the magnitude of this field was chosen by calculating dayside equatorial averages of the empirical field models of Alexeev and Belenkaya (2005) and Alexeev et al. (2006), and it varied with model magnetodisc radius $R_{\rm D}$ (see Achilleos et al., 2010a, Figure 6). In particular the component of the shielding field associated with the magnetopause currents was based on a dipole approximation of the magnetospheric magnetic field. In Chapter **??** we update this calculation for a more realistic magnetodisc magnetic field, and in Chapter **??** we modify this calculation using local time sector averages of the models of Alexeev and Belenkaya (2005) and Alexeev et al. (2006), to account for the increased significance of the tail current field compared to the magnetopause current field for nightside local time sectors. More details are given in those chapters.

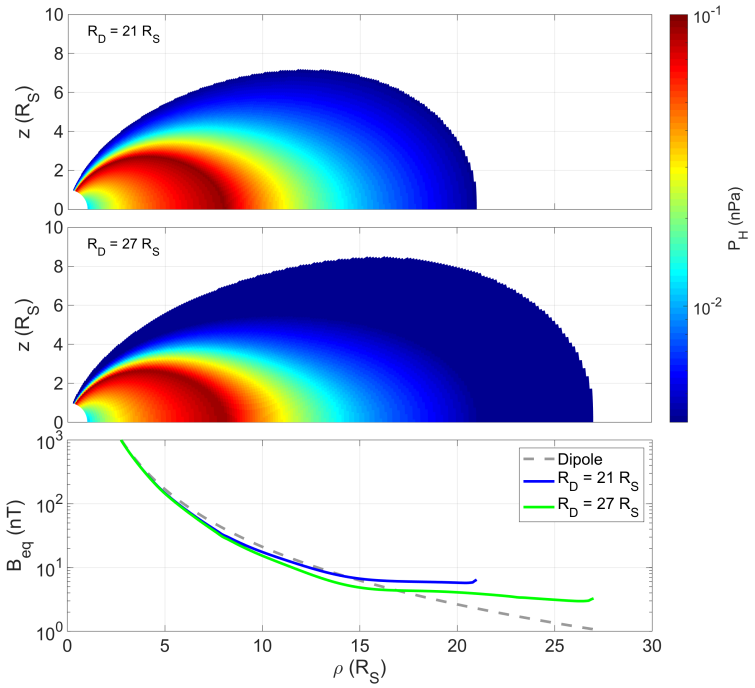

Figure 1.6: (a,b) Hot plasma pressure $P_{\rm H}$ predicted by the UCL/AGA magnetodisc model for models with different disc radii $R_{\rm D} = 21$ and $27\,{\rm R_S}$ respectively, as a function of cylindrical coordinates ρ and z, shown on a colour scale as per the colourbar. (c) Radial profiles of equatorial magnetic field strength for each of the two models, as shown by the legend, with dipole magnetic field profile shown by the grey dashed line for comparison.

Outputs from the UCL/AGA magnetodisc model for two configurations are shown in Figure 1.6, calculated with magnetopause radii $21\,R_S$ and $27\,R_S$ respectively, in line with the previously mentioned bimodal distribution in magnetopause stand-off distances observed by Achilleos et al. (2008); Pilkington et al. (2015a). In both models we use $K_H = 1 \times 10^6\,Pa\,m\,T^{-1}$ to represent typical conditions at Saturn. The top and middle panels show the distribution of hot plasma pressure; as this quantity is constant along magnetic field lines, colour contours exactly follow the magnetic field structure in the models. The bottom panel shows the equatorial profiles of total magnetic field strength for each model, compared to a dipole magnetic field. This figure shows how the UCL/AGA model predicts a more disc-like magnetic field structure, with more radially stretched field lines particularly in the middle magnetosphere, for a more expanded system, as expected from discussions in Section 1.4. The same information for a more expanded and wider range of system sizes is shown in Figure **??** in Chapter **??**, following adaptations and parameterisations discussed in that chapter.

1.6 Open Questions About Saturn's Magnetosphere: Motivations and Summary of this Thesis

As a community, we are still trying to understand the large-scale structure of Saturn's magnetosphere, and how it varies in response to internal and external influences. We know that the rapid planetary rotation rate, significant internal hot and cold plasma populations, and external solar wind conditions all play a role in determining the configuration of the magnetosphere – but which factor is dominant, and does this relationship change under different conditions and in different places?

The answers to these questions have consequences for other areas of magnetospheric physics at Saturn. In Sections 1.3.2 and 1.4.2 we touched on the concept of magnetospheric compressibility, and how the size of the magnetosphere scales with varying solar wind dynamic pressure. From equation (1.24), it can be seen that the relative magnitudes of the magnetic and plasma pressures just inside the magnetopause are important in determining this pressure balance, and hence the system size. Therefore an investigation of the magnetospheric compressibility, and how it varies under different conditions, can reveal information about overall pressure bal-

ance within the magnetosphere. In Chapter **??** we investigate this compressibility using the UCL/AGA magnetodisc model calculated at different system sizes. This approach complements previous observational studies based on *Cassini* data, and also provides an opportunity to explicitly investigate the influence of the variable hot plasma population on the compressibility behaviour. We also use our results to make a direct comparison with the compressibility of Jupiter's magnetosphere, to test our expectations that Saturn behaves as an intermediate between Earth and Jupiter.

The structure of Saturn's magnetodisc, and in particular the equatorial current sheet, also has consequences for understanding the periodic perturbations in Saturn's magnetic field. We discussed in Section 1.4.1 how Saturn's current sheet is observed to both 'flap' and 'breathe' periodically, at approximately the planetary rotation rate, due to rotating hemispheric magnetic perturbations. Research in this area is ongoing in the community, using both *Cassini* data analysis and MHD modelling approaches. In Chapter **??** we attempt to model these two periodic behaviours simultaneously, using the UCL/AGA magnetodisc model at different sizes to characterise the configuration of the magnetodisc at different phases of the planetary rotation. This allows us to provide an insight into how the breathing behaviour manifests in the *Cassini* magnetic field observations, and utilises the knowledge gained in the previous chapter of this thesis, about how magnetospheric structure varies with system size. For the flapping motion, we use a geometric model of a tilted and rippled current sheet from Arridge et al. (2011), and fit our combined model to *Cassini* magnetic field observations, in order to investigate how the behaviour varies over time and under different conditions.

In addition, we still do not have a complete picture of how the large-scale structure of Saturn's magnetosphere varies across magnetic local time. In particular the dawn/dusk asymmetry in the magnetic field configuration is not well constrained. This is in part due to relatively poor sampling of the dawn sector near the equator for much of the *Cassini* space mission, and the generally smaller scale asymmetries between the two sectors compared to noon/night, although recent results from MHD simulations have provided some insights (e.g. Jia and Kivelson, 2016). It is important to investigate local time asymmetry in the magnetospheric magnetic field structure

as this has consequences for other magnetic phenomena at Saturn, such as the location of the main auroral oval, and the aforementioned periodic modulation in the current sheet thickness. Therefore in Chapter **??** we investigate this local time variation by modifying the UCL/AGA model to characterise four different local time sectors, using more recent *Cassini* observations as boundary conditions to improve our characterisation of local times beyond noon.

Finally, in Chapter **??** we summarise the key results of the work presented in this thesis, and suggest avenues for future research that can best utilise these results, in order to continue our pursuit of understanding the configuration of Saturn's magnetosphere.

But first, we must discuss in more depth the other tool we use to investigate Saturn's magnetosphere; the *Cassini-Huygens* space mission to Saturn.

Bibliography

Achilleos, N., Arridge, C., Bertucci, C., Jackman, C., Dougherty, M., Khurana, K., and Russell, C. (2008). Large-scale dynamics of Saturn's magnetopause: Observations by Cassini. *Journal of Geophysical Research: Space Physics*, 113:A11209, DOI: 10.1029/2008JA013265.

Achilleos, N., Bertucci, C., Russell, C. T., Hospodarsky, G. B., Rymer, A. M., Arridge, C. S., et al. (2006). Orientation, location, and velocity of Saturn's bow shock: Initial results from the Cassini spacecraft. *Journal of Geophysical Research: Space Physics*, 111:A03201, DOI: 10.1029/2005JA011297, http://dx.doi.org/10.1029/2005JA011297.

Achilleos, N., Guio, P., and Arridge, C. S. (2010a). A model of force balance in Saturn's magnetodisc. *Monthly Notices of the Royal Astronomical Society*, 401:2349–2371, DOI: 10.1111/j.1365-2966.2009.15865.x.

Achilleos, N., Guio, P., Arridge, C. S., Sergis, N., Wilson, R., Thomsen, M., and Coates, A. J. (2010b). Influence of hot plasma pressure on the global structure of Saturn's magnetodisk. *Geophysical Research Letters*, 37:L20201, DOI: 10.1029/2010GL045159.

Alexeev, I. and Belenkaya, E. (2005). Modeling of the Jovian magnetosphere. *Annales Geophysicae*, 23:809–826, DOI: 10.5194/angeo-23-809-2005.

Alexeev, I. I., Kalegaev, V. V., Belenkaya, E. S., Bobrovnikov, S. Y., Bunce, E. J., Cowley, S. W. H., and Nichols, J. D. (2006). A global magnetic model of Saturn's magnetosphere and a comparison with Cassini SOI data. *Geophysical Research Letters*, 33:L08101, L08101, DOI: 10.1029/2006GL025896.

Andrews, D. J., Bunce, E. J., Cowley, S. W. H., Dougherty, M. K., Provan, G., and

Southwood, D. J. (2008). Planetary period oscillations in Saturn's magnetosphere: Phase relation of equatorial magnetic field oscillations and Saturn kilometric radiation modulation. *Journal of Geophysical Research: Space Physics*, 113:A09205, A09205, DOI: 10.1029/2007JA012937.

Andrews, D. J., Cowley, S. W. H., Dougherty, M. K., and Provan, G. (2010). Magnetic field oscillations near the planetary period in Saturn's equatorial magnetosphere: Variation of amplitude and phase with radial distance and local time. *Journal of Geophysical Research: Space Physics*, 115:A04212, A04212, DOI: 10.1029/2009JA014729.

Arridge, C., Russell, C., Khurana, K., Achilleos, N., Cowley, S., Dougherty, M., et al. (2008). Saturn's magnetodisc current sheet. *Journal of Geophysical Research: Space Physics*, 113:A04214, DOI: 10.1029/2007JA012540.

Arridge, C. S., André, N., Khurana, K., Russell, C., Cowley, S., Provan, G., et al. (2011). Periodic motion of saturn's nightside plasma sheet. *Journal of Geophysical Research: Space Physics*, 116:A11205, DOI: 10.1029/2011JA016827.

Bagenal, F., Adriani, A., Allegrini, F., Bolton, S. J., Bonfond, B., Bunce, E. J., et al. (2014). Magnetospheric Science Objectives of the Juno Mission. *Space Science Reviews*, 213:219–287, DOI: 10.1007/s11214-014-0036-8.

Bagenal, F. and Delamere, P. A. (2011). Flow of mass and energy in the magnetospheres of Jupiter and Saturn. *Journal of Geophysical Research: Space Physics*, 116:A05209, DOI: 10.1029/2010JA016294.

Bame, S. J., Barraclough, B. L., Feldman, W. C., Gisler, G. R., Gosling, J. T., McComas, D. J., et al. (1992). Jupiter's Magnetosphere: Plasma Description from the Ulysses Flyby. *Science*, 257:1539–1543, DOI: 10.1126/science.257.5076.1539.

Berchem, J. and Russell, C. T. (1982). The thickness of the magnetopause current layer - ISEE 1 and 2 observations. *Journal of Geophysical Research*, 87:2108–2114, DOI: 10.1029/JA087iA04p02108.

Bunce, E., Cowley, S., Alexeev, I., Arridge, C., Dougherty, M., Nichols, J., and Russell, C. (2007). Cassini observations of the variation of Saturn's ring current

parameters with system size. *Journal of Geophysical Research: Space Physics*, 112:A10202, DOI: 10.1029/2007JA012275.

Bunce, E. J., Arridge, C. S., Cowley, S. W. H., and Dougherty, M. K. (2008). Magnetic field structure of Saturn's dayside magnetosphere and its mapping to the ionosphere: Results from ring current modeling. *Journal of Geophysical Research: Space Physics*, 113:A02207, A02207, DOI: 10.1029/2007JA012538.

Burch, J. L., DeJong, A. D., Goldstein, J., and Young, D. T. (2009). Periodicity in Saturn's magnetosphere: Plasma cam. *Geophysical Research Letters*, 36:L14203, L14203, DOI: 10.1029/2009GL039043.

Carbary, J. F. and Mitchell, D. G. (2013). Periodicities in Saturn's magnetosphere. *Reviews of Geophysics*, 51:1–30, DOI: 10.1002/rog.20006.

Caudal, G. (1986). A self-consistent model of Jupiter's magnetodisc including the effects of centrifugal force and pressure. *Journal of Geophysical Research: Space Physics*, 91(A4):4201–4221.

Chapman, S. and Ferraro, V. C. A. (1930). A New Theory of Magnetic Storms. *Nature*, 126:129–130, DOI: 10.1038/126129a0.

Clarke, K. E., Andrews, D. J., Arridge, C. S., Coates, A. J., and Cowley, S. W. H. (2010). Magnetopause oscillations near the planetary period at Saturn: Occurrence, phase, and amplitude. *Journal of Geophysical Research: Space Physics*, 115:A08209, A08209, DOI: 10.1029/2009JA014745.

Connerney, J. E. P., Acuna, M. H., and Ness, N. F. (1981). Saturn's ring current and inner magnetosphere. *Nature*, 292:724–726, DOI: 10.1038/292724a0.

Connerney, J. E. P., Acuna, M. H., and Ness, N. F. (1983). Currents in Saturn's magnetosphere. *Journal of Geophysical Research*, 88:8779–8789, DOI: 10.1029/JA088iA11p08779.

Cowley, S. W. H., Badman, S. V., Bunce, E. J., Clarke, J. T., Gérard, J.-C., Grodent, D., et al. (2005). Reconnection in a rotation-dominated magnetosphere and its relation to saturn's auroral dynamics. *Journal of Geophysical*

Research: Space Physics, 110:A02201, DOI: 10.1029/2004JA010796, https://agupubs.onlinelibrary.wiley.com/doi/abs/10.1029/2004JA010796.

Cowling, T. G. (1933). The magnetic field of sunspots. *Monthly Notices of the Royal Astronomical Society*, 94:39–48.

Desch, M. D. and Kaiser, M. L. (1981). Voyager measurement of the rotation period of Saturn's magnetic field. *Geophysical Research Letters*, 8:253–256, DOI: 10.1029/GL008i003p00253.

Dougherty, M., Khurana, K., Neubauer, F., Russell, C., Saur, J., Leisner, J., and Burton, M. (2006). Identification of a dynamic atmosphere at Enceladus with the Cassini magnetometer. *Science*, 311(5766):1406–1409, DOI: 10.1126/science.1120985.

Dougherty, M. K., Cao, H., Khurana, K. K., Hunt, G. J., Provan, G., Kellock, S., et al. (2018). Saturn's magnetic field revealed by the Cassini Grand Finale. *Science*, 362(6410), ISSN: 0036-8075, DOI: 10.1126/science.aat5434, http://science.sciencemag.org/content/362/6410/eaat5434.

Dungey, J. W. (1961). Interplanetary Magnetic Field and the Auroral Zones. *Physical Review Letters*, 6:47–48, DOI: 10.1103/PhysRevLett.6.47.

Espinosa, S. A. and Dougherty, M. K. (2000). Periodic perturbations in Saturn's magnetic field. *Geophysical Research Letters*, 27:2785–2788, DOI: 10.1029/2000GL000048.

Espinosa, S. A., Southwood, D. J., and Dougherty, M. K. (2003). How can Saturn impose its rotation period in a noncorotating magnetosphere? *Journal of Geophysical Research: Space Physics*, 108:1086, 1086, DOI: 10.1029/2001JA005084.

Forsyth, C., Arridge, C. S., Milan, S. E., and Walsh, A. P. (2010). Magnetotails throughout the solar system. *Astronomy & Geophysics*, 51(6):6.28–6.30, DOI: 10.1111/j.1468-4004.2010.51628.x, http://dx.doi.org/10.1111/j.1468-4004.2010.51628.x.

Gurnett, D. A., Kurth, W. S., Hospodarsky, G. B., Persoon, A. M., Averkamp, T. F., Cecconi, B., et al. (2005). Radio and Plasma Wave Observations at

Saturn from Cassini's Approach and First Orbit. *Science*, 307:1255–1259, DOI: 10.1126/science.1105356.

Gurnett, D. A., Lecacheux, A., Kurth, W. S., Persoon, A. M., Groene, J. B., Lamy, L., et al. (2009). Discovery of a north-south asymmetry in Saturn's radio rotation period. *Geophysical Research Letters*, 36:L16102, L16102, DOI: 10.1029/2009GL039621.

Hansen, K., Ridley, A., Hospodarsky, G., Achilleos, N., Dougherty, M., Gombosi, T., and Tóth, G. (2005). Global MHD simulations of Saturn's magnetosphere at the time of Cassini approach. *Geophysical Research Letters*, 32:L20S06, DOI: 10.1029/ 2005GL022835.

Hathaway, D. H. (2015). The Solar Cycle. *Living Reviews in Solar Physics*, 12:4, 4, DOI: 10.1007/lrsp-2015-4.

Hunt, G. J., Cowley, S. W. H., Provan, G., Bunce, E. J., Alexeev, I. I., Belenkaya, E. S., et al. (2014). Field-aligned currents in Saturn's southern nightside magnetosphere: Subcorotation and planetary period oscillation components. *Journal of Geophysical Research: Space Physics*, 119:9847–9899, DOI: 10.1002/2014JA020506.

Jia, X. and Kivelson, M. G. (2012). Driving Saturn's magnetospheric periodicities from the upper atmosphere/ionosphere: Magnetotail response to dual sources. *Journal of Geophysical Research: Space Physics*, 117:A11219, A11219, DOI: 10.1029/2012JA018183.

Jia, X. and Kivelson, M. G. (2016). Dawn-dusk asymmetries in rotating magnetospheres: Lessons from modeling Saturn. *Journal of Geophysical Research: Space Physics*, 121:1413–1424, DOI: 10.1002/2015JA021950.

Kanani, S., Arridge, C. S., Jones, G., Fazakerley, A., McAndrews, H., Sergis, N., et al. (2010). A new form of Saturn's magnetopause using a dynamic pressure balance model, based on in situ, multi-instrument Cassini measurements. *Journal of Geophysical Research: Space Physics*, 115:A06207, DOI: 10.1029/2009JA014262.

Kane, M., Mitchell, D. G., Carbary, J. F., Krimigis, S. M., and Crary, F. J. (2008). Plasma convection in Saturn's outer magnetosphere determined from ions detected by the Cassini INCA experiment. *Geophysical Research Letters*, 35:L04102, L04102, DOI: 10.1029/2007GL032342.

Kellett, S., Bunce, E. J., Coates, A. J., and Cowley, S. W. H. (2009). Thickness of Saturn's ring current determined from north-south Cassini passes through the current layer. *Journal of Geophysical Research: Space Physics*, 114:A04209, A04209, DOI: 10.1029/2008JA013942.

Khurana, K. K. and Kivelson, M. G. (1989). On Jovian plasma sheet structure. *Journal of Geophysical Research: Space Physics*, 94(A9):11791–11803.

Kivelson, M. G. and Bagenal, F. (2014). Planetary Magnetospheres. In Spohn, T., Breuer, D., and Johnson, T. V., editors, *Encyclopedia of the Solar System*, pages 137–157. Elsevier, Boston, 3rd edition, DOI: https://doi.org/10.1016/B978-0-12-415845-0.00007-4.

Krimigis, S. M., Sergis, N., Mitchell, D. G., Hamilton, D. C., and Krupp, N. (2007). A dynamic, rotating ring current around Saturn. *Nature*, 450:1050–1053, DOI: 10.1038/nature06425.

Lecacheux, A., Galopeau, P., and Aubier, M. (1997). Re-visiting Saturnian Kilometric Radiation with Ulysses/URAP. In Rucker, H. O., Bauer, S. J., and Lecacheux, A., editors, *Planetary Radio Emission IV*, pages 313–325.

Masters, A., Mitchell, D., Coates, A., and Dougherty, M. (2011). Saturn's low-latitude boundary layer: 1. Properties and variability. *Journal of Geophysical Research: Space Physics*, 116:A06210, DOI: 10.1029/2010JA016421.

Mauk, B., Mitchell, D., McEntire, R., Paranicas, C., Roelof, E., Williams, D., et al. (2004). Energetic ion characteristics and neutral gas interactions in Jupiter's magnetosphere. *Journal of Geophysical Research: Space Physics*, 109:A09S12, DOI: 10.1029/2003JA010270.

McAndrews, H. J., Thomsen, M. F., Arridge, C. S., Jackman, C. M., Wilson, R. J., Henderson, M. G., et al. (2009). Plasma in Saturn's nightside magnetosphere and

the implications for global circulation. *Planetary and Space Science*, 57:1714–1722, DOI: 10.1016/j.pss.2009.03.003.

Milan, S. E., Provan, G., and Hubert, B. (2007). Magnetic flux transport in the Dungey cycle: A survey of dayside and nightside reconnection rates. *Journal of Geophysical Research: Space Physics*, 112:A01209, A01209, DOI: 10.1029/2006JA011642.

Morooka, M. W., Modolo, R., Wahlund, J.-E., André, M., Eriksson, A. I., Persoon, A. M., et al. (2009). The electron density of Saturn's magnetosphere. *Annales Geophysicae*, 27:2971–2991, DOI: 10.5194/angeo-27-2971-2009.

Odstrcil, D. and Pizzo, V. J. (1999). Distortion of the interplanetary magnetic field by three-dimensional propagation of coronal mass ejections in a structured solar wind. *Journal of Geophysical Research: Space Physics*, 104(A12):28225–28239, DOI: 10.1029/1999JA900319, https://agupubs.onlinelibrary.wiley.com/doi/abs/10.1029/1999JA900319.

Paranicas, C., Mitchell, D. G., Roelof, E. C., Brandt, P. C., Williams, D. J., Krimigis, S. M., and Mauk, B. H. (2005). Periodic intensity variations in global ENA images of Saturn. *Geophysical Research Letters*, 32:L21101, L21101, DOI: 10.1029/2005GL023656.

Parker, E. N. (1958). Dynamics of the Interplanetary Gas and Magnetic Fields. *Astrophysical Journal*, 128:664, DOI: 10.1086/146579.

Petrinec, S. and Russell, C. (1997). Hydrodynamic and MHD equations across the bow shock and along the surfaces of planetary obstacles. *Space Science Reviews*, 79(3-4):757–791.

Pilkington, N. M., Achilleos, N., Arridge, C. S., Guio, P., Masters, A., Ray, L., et al. (2015a). Internally driven large-scale changes in the size of Saturn's magnetosphere. *Journal of Geophysical Research: Space Physics*, 120:7289–7306, DOI: 10.1002/2015JA021290.

Provan, G., Andrews, D. J., Arridge, C. S., Coates, A. J., Cowley, S. W. H., Cox, G., et al. (2012). Dual periodicities in planetary-period magnetic field oscillations

in Saturn's tail. *Journal of Geophysical Research: Space Physics*, 117:A01209, A01209, DOI: 10.1029/2011JA017104.

Provan, G., Cowley, S. W. H., and Nichols, J. D. (2009). Phase relation of oscillations near the planetary period of Saturn's auroral oval and the equatorial magnetospheric magnetic field. *Journal of Geophysical Research: Space Physics*, 114:A04205, A04205, DOI: 10.1029/2008JA013988.

Ramer, K. M., Kivelson, M. G., Sergis, N., Khurana, K. K., and Jia, X. (2017). Spinning, breathing, and flapping: Periodicities in Saturn's middle magnetosphere. *Journal of Geophysical Research: Space Physics*, 122:393–416, DOI: 10.1002/2016JA023126.

Robbins, D. E., Hundhausen, A. J., and Bame, S. J. (1970). Helium in the solar wind. *Journal of Geophysical Research*, 75:1178, DOI: 10.1029/JA075i007p01178.

Russell, C. T., Luhmann, J. G., and Strangeway, R. J. (2016). *Space Physics: An Introduction*. Cambridge University Press.

Scarf, F. L., Kurth, W. S., Gurnett, D. A., Bridge, H. S., and Sullivan, J. D. (1981). Jupiter tail phenomena upstream from Saturn. *Nature*, 292:585, DOI: 10.1038/292585a0.

Schneider, O. (1967). Interaction of the Moon with the Earth's Magnetosphere. *Space Science Reviews*, 6:655–704, DOI: 10.1007/BF00168794.

Sergis, N., Achilleos, N., Guio, P., Arridge, C., Sorba, A., Roussos, E., et al. (2018). Mapping Saturn's Night Side Plasma Sheet Using Cassini's Proximal Orbits. *Geophysical Research Letters*, 45, DOI: 10.1029/2018GL078141.

Sergis, N., Jackman, C. M., Thomsen, M. F., Krimigis, S. M., Mitchell, D. G., Hamilton, D. C., et al. (2017). Radial and local time structure of the Saturnian ring current, revealed by Cassini. *Journal of Geophysical Research: Space Physics*, 122:1803–1815, DOI: 10.1002/2016JA023742.

Sergis, N., Krimigis, S., Mitchell, D., Hamilton, D., Krupp, N., Mauk, B., et al. (2007). Ring current at Saturn: Energetic particle pressure in Saturn's equato-

rial magnetosphere measured with Cassini/MIMI. *Geophysical Research Letters*, 34:L09102, DOI: 10.1029/2006GL029223.

Sergis, N., Krimigis, S., Mitchell, D., Hamilton, D., Krupp, N., Mauk, B., et al. (2009). Energetic particle pressure in Saturn's magnetosphere measured with the Magnetospheric Imaging Instrument on Cassini. *Journal of Geophysical Research: Space Physics*, 114:A02214, DOI: 10.1029/2008JA013774.

Sergis, N., Krimigis, S., Roelof, E., Arridge, C. S., Rymer, A., Mitchell, D., et al. (2010). Particle pressure, inertial force, and ring current density profiles in the magnetosphere of Saturn, based on Cassini measurements. *Geophysical Research Letters*, 37:L02102, DOI: 10.1029/2009GL041920.

Slavin, J., Smith, E., Spreiter, J., Stahara, S., et al. (1985). Solar wind flow about the outer planets- Gas dynamic modeling of the Jupiter and Saturn bow shocks. *Journal of Geophysical Research*, 90:6275–6286.

Smith, C. G. A., Ray, L. C., and Achilleos, N. A. (2016). A planetary wave model for Saturn's 10.7-h periodicities. *Icarus*, 268:76–88, DOI: 10.1016/j.icarus.2015.12.041.

Smith, E. J., Davis, L., Jones, D. E., Coleman, P. J., Colburn, D. S., Dyal, P., and Sonett, C. P. (1980). Saturn's magnetic field and magnetosphere. *Science*, 207:407–410, DOI: 10.1126/science.207.4429.407.

Southwood, D. J. and Cowley, S. W. H. (2014). The origin of Saturn's magnetic periodicities: Northern and southern current systems. *Journal of Geophysical Research: Space Physics*, 119:1563–1571, DOI: 10.1002/2013JA019632.

Southwood, D. J. and Kivelson, M. G. (1989). Magnetospheric interchange motions. *Journal of Geophysical Research*, 94:299–308, DOI: 10.1029/JA094iA01p00299.

Spreiter, J. R., Alksne, A. Y., and Abraham-Shrauner, B. (1966). Theoretical proton velocity distributions in the flow around the magnetosphere. *Planetary and Space Science*, 14:1207–1220, DOI: 10.1016/0032-0633(66)90033-X.

Tokar, R., Johnson, R., Hill, T., Pontius, D., Kurth, W., Crary, F., et al. (2006).

The interaction of the atmosphere of Enceladus with Saturn's plasma. *Science*, 311(5766):1409–1412, DOI: 10.1126/science.1121061.

Vasyliunas, V. (1983). Plasma distribution and flow. *Physics of the Jovian magnetosphere*, 1:395–453.

Warren, H. P. and Brooks, D. H. (2009). The Temperature and Density Structure of the Solar Corona. I. Observations of the Quiet Sun with the EUV Imaging Spectrometer on Hinode. *The Astrophysical Journal*, 700(1):762, http://stacks.iop.org/0004-637X/700/i=1/a=762.

Wilson, R., Tokar, R., Henderson, M., Hill, T., Thomsen, M., and Pontius, D. (2008). Cassini plasma spectrometer thermal ion measurements in Saturn's inner magnetosphere. *Journal of Geophysical Research: Space Physics*, 113:A12218, DOI: 10.1029/2008JA013486.

Wilson, R. J., Bagenal, F., and Persoon, A. M. (2017). Survey of thermal plasma ions in Saturn's magnetosphere utilizing a forward model. *Journal of Geophysical Research: Space Physics*, 122:7256–7278, DOI: 10.1002/2017JA024117.